ACS APPLIED MATERIALS & INTERFACES

Research Article

www.acsami.org

Photovoltaic Performance and Interface Behaviors of Cu(In,Ga)Se_2 Solar Cells with a Sputtered-Zn(O,S) Buffer Layer by High-Temperature Annealing

Jae-Hyung Wi,[†] Tae Gun Kim,[‡,§] Jeong Won Kim,[‡,§] Woo-Jung Lee,[†] Dae-Hyung Cho,[†] Won Seok Han,[†] and Yong-Duck Chung*[,†,‡]

[†]Electronics and Telecommunications Research Institute (ETRI), 218 Gajeong-ro, Yuseong-gu, Daejeon 305-700, Republic of Korea

[‡]Korea University of Science and Technology (UST), 217 Gajeong-ro, Yuseong-gu, Daejeon 305-350, Republic of Korea

[§]Korea Research Institute of Standards and Science (KRISS), 267 Gajeong-ro, Yuseong-gu, Daejeon 305-340, Republic of Korea

Supporting Information

ABSTRACT: We selected a sputtered-Zn(O,S) film as a buffer material and fabricated a Cu(In,Ga)Se_2 (CIGS) solar cell for use in monolithic tandem solar cells. A thermally stable buffer layer was required because it should withstand heat treatment during processing of top cell. Postannealing treatment was performed on a CIGS solar cell in vacuum at temperatures from 300−500 °C to examine its thermal stability. Serious device degradation particularly in V_{OC} was observed, which was due to the diffusion of thermally activated constituent elements. The elements In and Ga tend to out-diffuse to the top surface of the CIGS, while Zn diffuses into the interface of Zn(O,S)/CIGS. Such rearrangement of atomic fractions modifies the local energy band gap and band alignment at the interface. The notch-shape induced at the interface after postannealing could function as an electrical trap during electron transport, which would result in the reduction of solar cell efficiency.

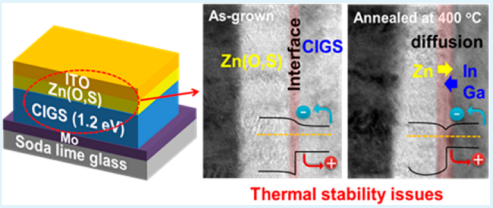

KEYWORDS: *Cu(In,Ga)Se_2, Zn(O,S), bottom cell, thermal annealing, depth profiling, energy band alignment*

INTRODUCTION

Technological research and development of thin film materials such as Cu(In,Ga)Se_2 (CIGS) have been continuously carried out for the photovoltaic market because of their outstanding features. These include high absorption coefficient, appropriate band gap, and band gap engineering. Recently, a CIGS-based single-junction solar cell achieved the highest known power conversion efficiency of 21.7%.[1] This record-breaking cell contains a CdS thin film grown by chemical bath deposition (CBD) as a buffer layer. However, the use of Cd can cause damage to the environment because it is a toxic heavy metal. Because of such environmental issues, there have been many investigations of Cd-free buffer layers in past decades. Among the Cd-free buffer layer materials studied, Zn-based materials such as ZnS,[2] Zn(O,S),[3−6] (Zn,Mg)O,[7] and (Zn,Sn)O[8] are considered reasonable alternatives to CdS[9] because they have the advantages of better thermal stability and short-wavelength gain.[10,11] Moreover, it is worthy of notice that CIGS tandem solar cells are subjected to heat treatment during fabrication of the top cell (e.g., $CuGaSe_2$).[12] For a feasible bottom cell in the 2-terminal monolithic tandem structure, we should prevent excessive diffusion of Zn or Cd from the buffer layer into the CIGS absorber layer. Thus, the buffer layer prepared on the CIGS absorber should be capable of withstanding the high temperatures. Also, physical vacuum deposition (PVD)-Zn-based buffer layer is more favorable due to lower diffusion rate than CBD-CdS or ZnS buffer layer.[13] The effects of annealing on CIGS solar cells with Zn-based buffer layer were previously investigated by several groups. Nakada et al. observed a buried p−n junction created by Zn diffusion into the CIGS thin film after heat treatment even at relatively low temperature. Moreover, they developed a new technique for forming a homojunction in CIGS thin-film solar cells by utilizing the above-mentioned Zn interdiffusion.[14] ZSW group demonstrated gain and loss of solar cell efficiency after annealing treatment on the basis of Zn diffusion.[15] Although it is clear that annealing effect is an important factor in solar cell performance, there are few systematic analyses or well-defined explanations about the mechanisms of degradation that occur after annealing treatment of CIGS solar cells with a Zn-based buffer layer.

In this study, we fabricated a CIGS solar cell with a sputtered-Zn(O,S) buffer layer. To investigate its feasibility as the bottom cell in the 2-terminal monolithic tandem structure, we performed postannealing treatment from 300−500 °C in vacuum. To examine its photovoltaic performance and interface behaviors, depth profile analysis was conducted on the Zn(O,S)/CIGS solar cell using secondary ion mass spectros-

Received: June 2, 2015
Accepted: July 20, 2015
Published: July 20, 2015

DOI: 10.1021/acsami.5b04815
ACS Appl. Mater. Interfaces 2015, 7, 17425−17432

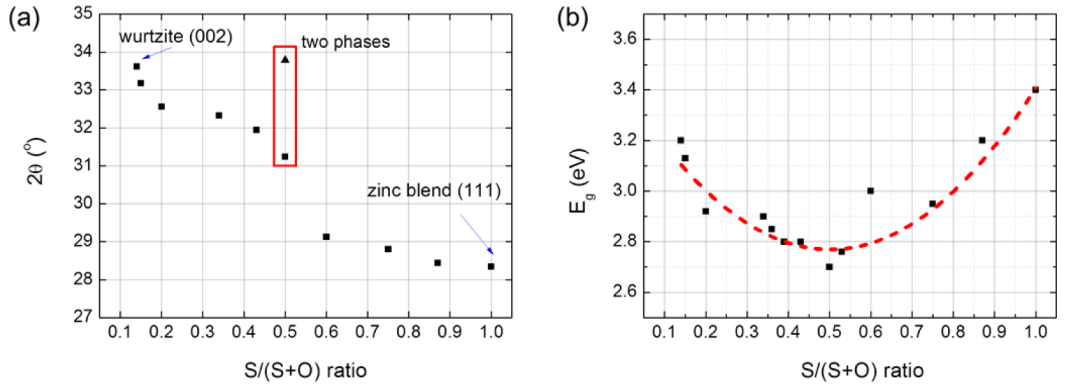

Figure 1. (a) XRD peak position of sputtered-$ZnO_{1-x}S_x$ with $0.14 \leq x \leq 1$. (b) Optical band gap (E_g) of $ZnO_{1-x}S_x$ films with $0.14 \leq x \leq 1$ (x is sulfur content). These figures refer to the XRD patterns and absorption spectra from transmission spectra of $ZnO_{1-x}S_x$ thin films in Supporting Information, Figure S1.

copy (SIMS), transmission electron microscopy (TEM), X-ray photoelectron spectroscopy (XPS), and ultraviolet/inverse photoemission spectroscopy (UPS/IPES).

EXPERIMENTAL SECTION

The devices were fabricated with a structure of soda lime glass (SLG)/Mo/CIGS/sputtered-Zn(O,S)/ITO/Ni/Al. A 900 nm layer of Mo was deposited on the SLG substrate by the DC-sputtering method. Then, 2.5 μm-thick CIGS absorber with Cu/(In+Ga) ratio = 0.97 and Ga/(Ga+In) ratio = 0.28 were deposited by the coevaporation method using a multistage process at a substrate temperature of 570 °C.[16] The 50 nm-thick Zn(O,S) layer was deposited by RF sputtering. The ZnS target (4") was used with RF power of 150 W, and then an argon/oxygen mixture gas (Ar 90%/O_2 10%) was introduced at a steady total gas flow rate of 100 sccm. The substrate temperature was fixed at 200 °C. The base pressure and working pressure were 1.2×10^{-7} Torr and 20 mTorr, respectively. To characterize the structure and optical properties of the Zn(O,S) layer in Figure 1, the 100 nm-thick Zn(O,S) thin films were grown on the SLG. The S/(S+O) ratio was changed by varying the oxygen partial pressure, O_2 = [O_2 (0.1−1) sccm/(Ar (99.9−99) sccm + O_2 (0.1−1) sccm)] × 100 from 0.1−1% with fixed ZnS sputter power. To prepare the ITO films, we used a sintered ceramic target of 99.99%, In_2O_3/SnO_2 = 90:10 wt %. The target-to-substrate distance was 15 cm. The sputter deposition was done under the conditions of RF power, Ar flow, and an operating pressure of 100 W, 50 sccm, and 0.67 Pa, respectively. ITO films 150 nm-thick were deposited at 200 °C for 30 min.[17] In the case of the Zn(O,S)/CIGS solar cell, no i-ZnO was used to prevent thermally activated degradation, although the i-ZnO of the standard transparent conductive oxide (TCO) double layers could improve the open circuit voltage (V_{OC}).[18] Finally, we performed the deposition for the Ni/Al grid contact using thermal evaporation. The completed CIGS solar cells have an active area of 0.47 cm^2. To investigate the effects of annealing on the tandem solar cell, the CIGS solar cells were heated up to temperatures of 300−500 °C for 60 min in vacuum, and then their cell performance was characterized. X-ray Diffraction (XRD) with Cu Kα radiation (λ = 0.15406 nm) was used to characterize the crystalline structure of the Zn(O,S) thin films as a function of sulfur content. The S/(S+O) ratio of the Zn(O,S) films was detected by energy dispersive spectroscopy (EDS). An UV−vis−NIR (near-infrared) spectrophotometer was used to measure the optical band gap energy (E_g) of the Zn(O,S) thin films.

The current density (J)−voltage (V) characteristic of the annealed CIGS solar cells was measured under AM 1.5 spectrum for 1000 W/m^2 irradiance at room temperature. The external quantum efficiency (EQE) of the CIGS solar cells was also measured. A SIMS analysis was carried out to investigate the depth profile of the buffer element in CIGS thin film solar cells using O^{2+} primary ions. The acceleration voltage and the beam current of the primary source were 15 keV and 5 nA, respectively. The change in the thickness of the Zn(O,S) buffer layer on CIGS film after annealing was verified by TEM. The chemical state at the interface of Zn(O,S)/CIGS films after annealing was verified by XPS. To calculate the energy levels of the valence band (VB) and conduction band (CB) at the Zn(O,S)/CIGS interface, the valence band maximum (VBM) and the conduction band minimum (CBM) were measured using UPS and IPES, respectively. Those electron spectroscopy tools probe only a few nm of depth information. Depth profiles of the Zn(O,S)/CIGS layers were provided by Ar^+ sputtering at 2 keV, which gives a sputtering rate of 0.5−1.0 nm/min. Before each depth profiling, samples had been treated by mild sputtering at 0.35 keV for 10 min to remove surface contamination. The base pressure of the analysis chamber was maintained at 10^{-10} Torr. The UPS and XPS measurements were performed using a hemispherical electron energy analyzer with a charge-coupled device (CCD) camera (SES-100, VG-Scineta). The UPS measurement used He I ($h\omega$ = 21.22 eV) and He II ($h\omega$ = 40.8 eV) gas discharge lamps as excitation sources with sample bias of −10 V for the secondary electron cutoff region. The XPS measurement used an Al Kα ($h\omega$ = 1486.5 eV) without a monochromator. The energy resolutions were 0.1 and 1.0 eV for UPS and XPS, respectively. The IPES was measured in an isochromatic mode in using an ELS100 electron source (PSP Vacuum Technology) and BaF_2 window/KBr-coated MCP photon detector (PHOTONIS).[19,20] The energy resolution was 0.6 eV. The E_f was used as an energy reference that was calibrated using clean Au (111).

RESULTS AND DISCUSSION

The XRD phase transition and optical band gap (E_g) of the Zn(O,S) thin films as a function of sulfur content (it is expressed with $ZnO_{1-x}S_x$ in this figure) are shown in Figure 1, panels a and b. The $ZnO_{1-x}S_x$ films have a wurtzite structure with (002) preferential orientation on the oxygen-rich side and a zinc-blend structure with (111) preferential orientation on the sulfur-rich phase, as shown in Figure 1, panel a. The oxygen-rich phase (002), having relatively high diffraction angle (near 33.62°), shifted to a lower angle (near 28.34°) with increasing sulfur content. It is well-known that the zinc-blend structure is predominant and more stable than the wurtzite structure under ambient conditions.[21] The $ZnO_{1-x}S_x$ film, however, consists of two phases when the S/(S+O) ratio is 0.5 (Supporting Information, Figure S1). The composition range in which homogeneous alloys are formed depends not only on the growth temperature, but also probably on the specific technique used for preparation of the material (i.e., nonequilibrium effects play an important role).[22−24] The specific mechanisms for the zinc blend and wurtzite structure between the ZnS and ZnO have been proposed from the perspective of thermodynamic stability.[25]

DOI: 10.1021/acsami.5b04815
ACS Appl. Mater. Interfaces 2015, 7, 17425−17432

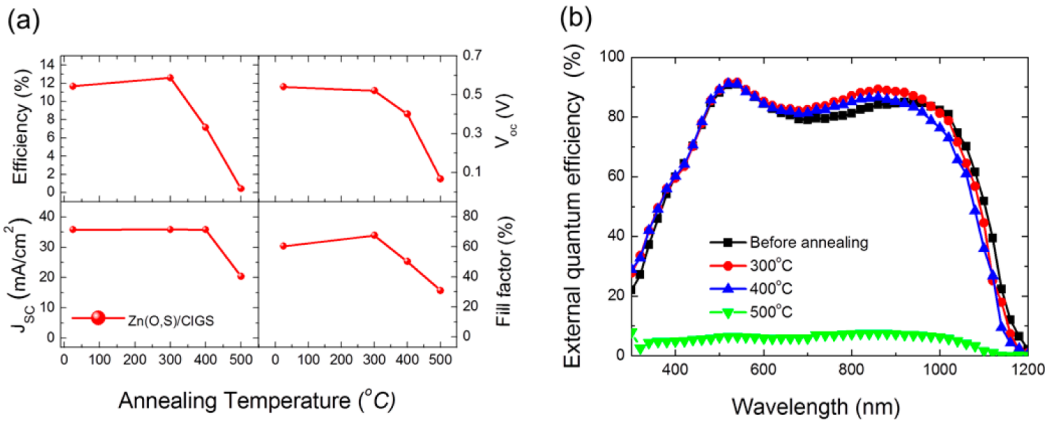

Figure 2. (a) The photovoltaic parameters and (b) EQE curves of CIGS solar cells with the sputtered-Zn(O,S) buffer layers before and after annealing at the temperatures from 300−500 °C for 60 min in vacuum.

Optical spectroscopy showed the dependence of the E_g on the sulfur content of $ZnO_{1-x}S_x$ thin films. The $ZnO_{1-x}S_x$ alloy film is referred to as a material with isovalent impurities. Because of isovalent impurities of oxygen and sulfur with a large mismatch in their electronegativity and atom size, $ZnO_{1-x}S_x$ films are expected to have E_g bowing effects.[26−28] From absorption measurements, the bowing parameter of the band gap was determined to be 3 eV. The E_g of wurtzite $ZnO_{1-x}S_x$ film decreased from 3.15 to 2.7 eV, and that of zinc blend $ZnO_{1-x}S_x$ film increased from 2.7 to 3.4 eV, with increasing sulfur content. For sputtered-$ZnO_{1-x}S_x$ films, the near band edge absorption became broad for highly alloyed films. Whether this effect is entirely related to the statistical occupation of the anion sites alone remains to be investigated.[27] Thus, $ZnO_{1-x}S_x$ alloy films have attracted intense interest as an alternative buffer layer due to controllable E_g engineering in the short-wavelength range, as compared to CdS. Generally, a $ZnO_{1-x}S_x$ buffer layer with a ZnO-rich phase in a device leads to lower V_{OC}, whereas that with a ZnS-rich phase blocks photocurrent by conduction band offset (CBO) between the CIGS absorber and Zn(O,S) buffer layer.[29]

To verify the influence of the relative concentration in devices, we fabricated a series of CIGS solar cells with a $ZnO_{1-x}S_x$ buffer layer, varying the S content (Supporting Information, Figure S2). According to our experimental results, the best cell efficiency could be obtained when $x = 0.43$ in the $ZnO_{1-x}S_x$ buffer layer. Thus, we will discuss the detailed results of the CIGS solar cell with a $ZnO_{0.57}S_{0.43}$ buffer layer. To examine the annealing effect on the CIGS solar cell, postannealing treatment was performed on the cells at temperatures from 300−500 °C.

Figure 2 shows the $J-V$ and EQE curves of the Zn(O,S)/CIGS solar cells as a function of the postannealing temperature. The solar cell performance rapidly deteriorated at the annealing temperature of 400 °C, as indicated in Figure 2, panel a. The as-fabricated CIGS solar cells efficiency was 11.68%. It was interesting that the cell efficiency improved from 11.68 to 12.61% at the annealing temperature of 300 °C. This was caused by a slight increase in fill factor (FF) from 60.4 to 67.5%. The EQE curves increased from 700 to 1000 nm and slightly decreased from 1000 to 1200 nm, as shown in Figure 2, panel b. From these results, the improved cell efficiency with increasing FF was attributed to the performance of TCO. The spectral transmittance of the annealed ITO film increases with varying carrier concentration and mobility.[17] The solar cell efficiency was drastically decreased to 7.16% with decreasing V_{OC} and FF at the annealing temperature of 400 °C despite retention of the same short circuit current (J_{SC}) value. The cause of the decrease in V_{OC} appeared to be recombination in the interface between the Zn(O,S) and CIGS layers, in connection with the decrease of EQE in the long wavelength region (Figure 2b). This is because a surface-buried junction could be formed at the Zn(O,S)/CIGS interface from the diffusion of Zn atoms.[3] When the annealing temperature was 500 °C, the current collection dramatically decreased over the full spectrum. The solar cell performance clearly exhibited annealing effects: degradation in the quality of its p−n junction at the annealing temperature of 400 °C. To identify the degree of Zn diffusion, SIMS depth profiles were analyzed for as-grown and 400 °C annealed Zn(O,S)/CIGS, as indicated in Figure 3.

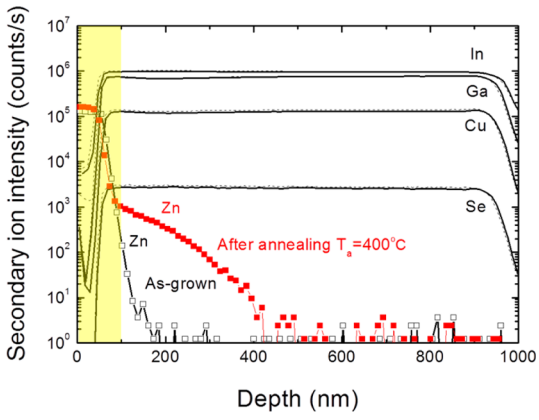

Figure 3. SIMS depth profiles of Zn content in the sputtered-Zn(O,S)/CIGS films after annealing at 400 °C.

The Zn atoms were actively diffused into the CIGS layer after the annealing treatment. The diffused Zn atoms acted as defects, such as Zn^{2+} being used as a substitute for Cu^+ and Cu vacancies, which generally contribute to recombination in the depletion region. According to previously reported results, the group II elements such as Zn and Cd can easily be diffused into the CIGS-based absorber, which converts junction properties from p-type to n-type due to the excessive Zn and Cd content after postannealing.[14] The widening of the depletion region implies a decrease in carrier concentration, resulting in a lower V_{OC} and hence decreased efficiency. The role of Zn diffusion in

DOI: 10.1021/acsami.5b04815
ACS Appl. Mater. Interfaces 2015, 7, 17425−17432

CIGS is that small amount of early diffusion enhances the cell performance and large amount of Zn diffusion degraded cell performance primarily due to losing V_{OC} and FF. These atomic diffusions in the opposite direction from that intended, as proved in SIMS depth profiles, can induce formation of a thick interfacial layer. This was confirmed by measuring TEM cross-sectional images for as-fabricated and 400 °C annealed Zn(O,S)/CIGS film. Figure 4, panel a clearly shows a Zn(O,S) layer about 50 nm thick before annealing. However, the interface became less abrupt with annealing, and the thickness of the interdiffusion layer increased to about 10 nm. The diffused interfacial layer can cause a recombination path and a CIGS-type conversion. To investigate the chemical state of the Zn(O,S)/CIGS interface, the XPS depth profile was measured as a function of Ar^+ sputtering time for as-grown and 400 °C annealed Zn(O,S)/CIGS films.

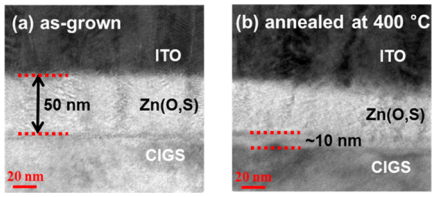

Figure 4. Cross-sectional TEM images of (a) as-grown ITO/Zn(O,S)/CIGS and (b) annealed ITO/Zn(O,S)/CIGS films at 400 °C for 60 min.

Figure 5 shows XPS core level spectra as a function of Ar^+ sputtering time for as-grown and 400 °C annealed Zn(O,S)/CIGS samples, respectively. The bracketed (x) or (x′) in Figures 5 and 6 indicate each series of spectra either for as-grown or for annealed samples. The top-layer elements for Zn(O,S) are presented in panels a–c (a′–c′), while the underlying layer elements of CIGS are presented in panels c–f (c′–f′). The S 2s and Se 3s core levels are both displayed in Figure 5, panels c and c′. In Figure 5, panels a and a′, the initial Zn $2p_{3/2}$ core level binding energy (BE) for an annealed sample appears at 1021.8 eV. This is 0.3 eV higher than that for the as-grown sample. However, with increased sputtering time, the Zn $2p_{3/2}$ peaks for both samples converged to 1022.0 eV, and their intensities gradually decreased. A difference in the initial core level BE values of O 1s and S 2s was also observed in the same manner. This consistent BE shift without any chemical difference indicates a slightly different energy level alignment upon annealing. The O 1s core level spectra in Figure 5, panel b shows an asymmetric line shape with a shoulder on the high BE side unlike the Zn $2p_{3/2}$ peak. Additionally, the O 1s peak for the annealed sample in Figure 5, panel b′ shows broader full width half-maximum (fwhm) than that for the as-grown one. Through O 1s peak-fitting, they turn out to be decomposed into two or three components with similar spectral width. The high BE shoulder (yellow–green solid) is attributed to $Zn(OH)_2$ compound.[30,31] This $Zn(OH)_2$ compound is rapidly removed over the progress of the sputtering. This result indicates that the $Zn(OH)_2$ component exists primarily on the topmost surface. The main peak (blue–green solid) about 1.7 eV lower than the $Zn(OH)_2$ peak is related to ZnO compound. The additional peak (pink solid) is unknown but probably due to other types of oxygen species bonded to Zn and In. Because the S 2p core level overlaps with Se 3p, the S 2s core level spectra in Figure 5, panel c are displayed to distinguish S and Se related peaks. Initial S 2s peaks for as-grown and annealed samples appeared at 225.9 and 226.1 eV, respectively. With more sputtering time, the initial singlet peaks changed to form a doublet. The new peak, which was located at a BE 3.2 eV higher

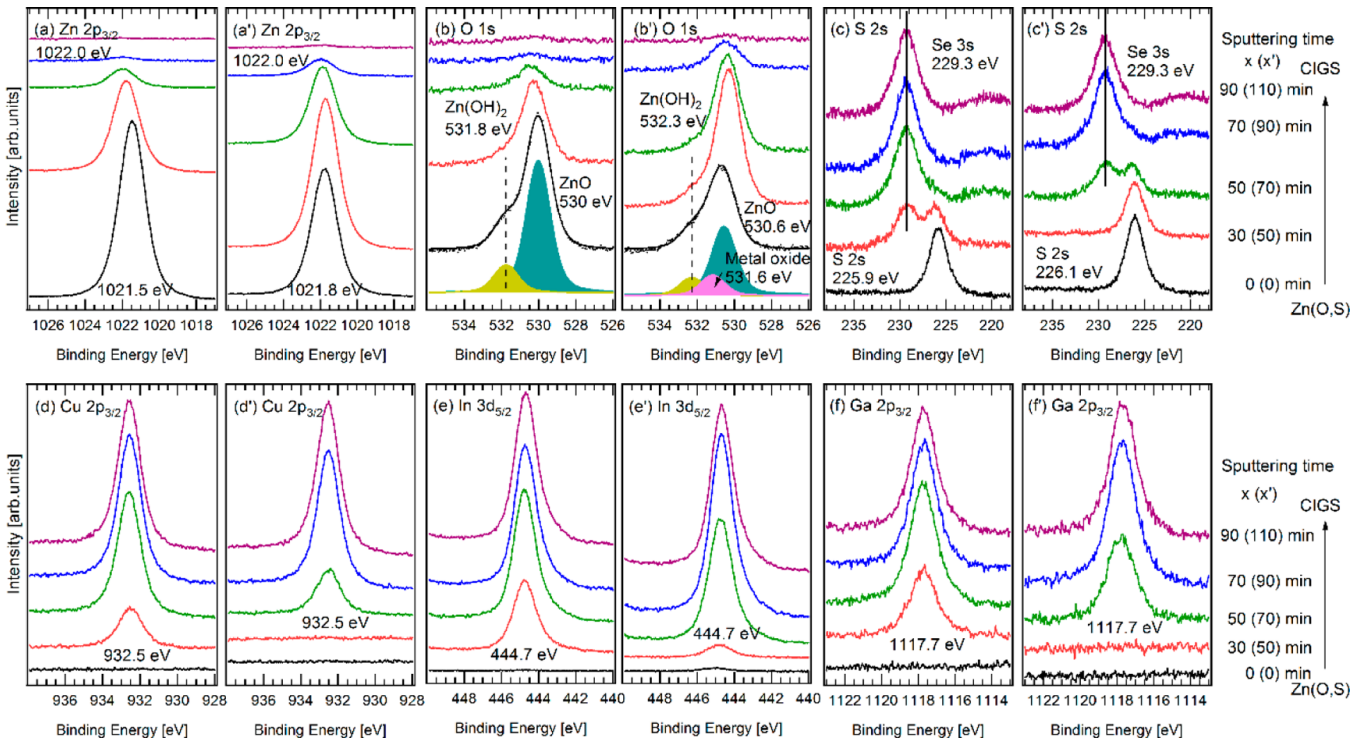

Figure 5. XPS spectra as a function of Ar^+ sputtering time for the as-grown Zn(O,S)/CIGS and for Zn(O,S)/CIGS annealed at 400 °C for 60 min. Each component of the core level spectra: Zn $2p_{3/2}$, O 1s, S 2s, Cu $2p_{3/2}$, In $3d_{3/2}$, and Ga $2p_{3/2}$, are displayed in panels a–f or a′–f′, respectively.

DOI: 10.1021/acsami.5b04815
ACS Appl. Mater. Interfaces 2015, 7, 17425–17432

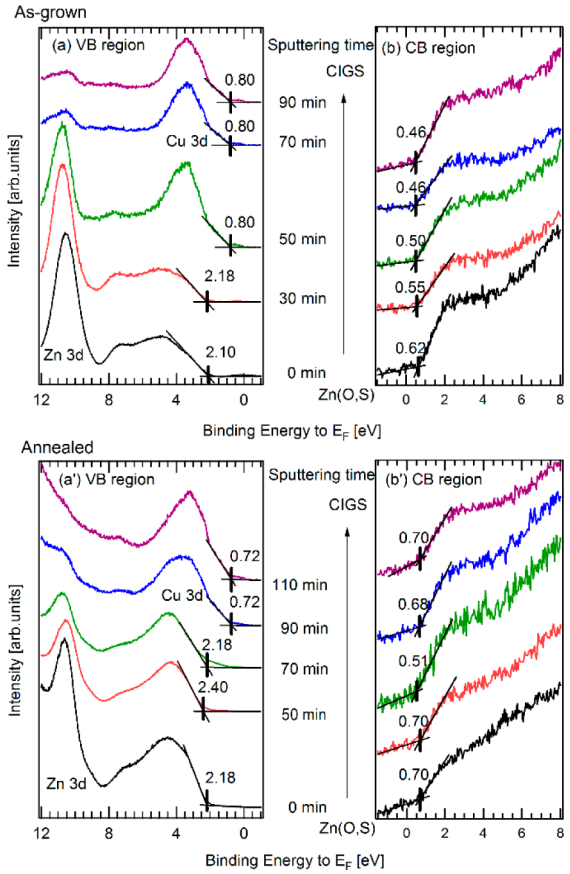

Figure 6. UPS and IPES spectra as a function of Ar^+ sputtering time for the as-grown Zn(O,S)/CIGS are displayed in panels a and b. Spectra for Zn(O,S)/CIGS annealed at 400 °C case are displayed in panels a′ and b′, respectively.

than the initial S 2s peak, is a Se 3s peak of the underlying CIGS layer. This appearance of a doublet shape enables the location of Zn(O,S)/CIGS interface. It can be inferred that the as-grown sample forms the interface at 30 min sputtering depth. However, after annealing, the interface became located at 70 min sputtering depth, which looks deeper than the as-grown case. That is, the annealing process made the Zn(O,S) layer thicker or the interface became located deeper due to interface diffusion. After further sputtering, the S 2s peak totally disappeared, and the Se 3s peak became dominant at 229.3 eV for both samples.

In Figure 5, panel e′, a small amount of In atoms could be detected on the top surface of the Zn(O,S) buffer layer after thermal annealing, which was absent on the as-grown film (Figure 5e). Such out-diffusion of In atoms (existing probably in the form of In_2O_3) is the result of thermodynamic factors because of the low surface energy of In. This out-diffusion behavior of constituents of the underlying layer at the annealing temperature could induce a perturbation of the electronic structure across the interface and thereby the solar cell performance. This is discussed in the following. On the other hand, Figure 5, panels c−f and c′−f′ show the Se 3s, Cu $2p_{3/2}$, In $3d_{5/2}$, and Ga $2p_{3/2}$ for the constituent elements of the underlying CIGS layer for both as-grown and annealed samples. Whether the sample was annealed or not, the BE of each atom was unchanged along the depth, which is a different trend from that shown by the elements in the Zn(O,S) layer. The constant core level peak positions of both CIGS layers mean that the valence band edges of both samples were very close to each other, which will be shown in the following. The left side of Table 1 summarizes the atomic stoichiometry of the Zn(O,S) layer, and the right side shows that of the CIGS layer for both as-grown and annealed samples above and below the table. Among them, the ratio S/(S+O) in Zn(O,S) is an important parameter in the determination of E_g.[22] The S/(S+O) ratios in the Zn(O,S) layer, in relation to sputtering time, and for as-grown and annealed samples were 0.35−0.37 and 0.23−0.51, respectively. In the case of the as-grown sample, the S/(S+O) ratio remained uniform, while it showed large variation for the annealed samples. This discrepancy comes from the relative oxygen diffusion into the CIGS caused by thermal annealing. Accordingly, the electronic band structure was influenced a lot by heat treatment (Figures 6 and 7).

The right side of Table 1 shows the atomic stoichiometry of the CIGS constituents. Both samples reveal a Cu-poor region at the Zn(O,S)/CIGS interface. There is about a 10% Cu deficiency compared to the Cu fraction in bulk CIGS. These Cu vacancies in Ga or In-rich phase generated the ordered defect compounds (ODC) that act as electron acceptors.[32] One striking difference between two samples is that the Ga fraction of the annealed CIGS layer was 1.85-times larger than that of

Table 1. Summary of the Elemental Stoichiometry Measured by XPS[a]

as-grown Zn(O,S)/CIGS								
sputtering time (min)	Zn $2p_{3/2}$	O 1s	S 2p	sputtering time (min)	Cu $2p_{3/2}$	In $3d_{5/2}$	Ga $2p_{3/2}$	Ga /(In+Ga)
0	57.9%	26.4%	15.7%	0				
30	53.9%	30.1%	16.0%	30	17.6%	25.3%	6.2%	19.7%
50	45.2%	35.5%	19.3%	50	26.2%	22.4%	5.6%	20.0%
70	37.2%	45.8%	17.0%	70	27.7%	22.3%	5.5%	19.8%
90				90	27.8%	23.3%	5.3%	18.5%
annealed Zn(O,S)/CIGS								
sputtering time (min)	Zn $2p_{3/2}$	O 1s	S 2p	Sputtering time (min)	Cu $2p_{3/2}$	In $3d_{5/2}$	Ga $2p_{3/2}$	Ga /(In+Ga)
0	54.8%	22.2%	22.9%	0		100.0%		
50	57.5%	29.2%	13.3%	50		100.0%		
70	50.5%	36.2%	13.3%	70	15.6%	33.2%	12.0%	26.5%
90	44.8%	44.4%	10.8%	90	24.0%	24.4%	10.4%	29.9%
110				110	26.9%	22.3%	9.8%	30.5%

[a]We focused on Cu, In, and Ga composition variation of the CIGS interface to verify Cu vacancies as well as In and Ga out-diffusion into the surface of CIGS. The Se element is numerically omitted assuming it is balanced.

DOI: 10.1021/acsami.5b04815
ACS Appl. Mater. Interfaces 2015, 7, 17425−17432

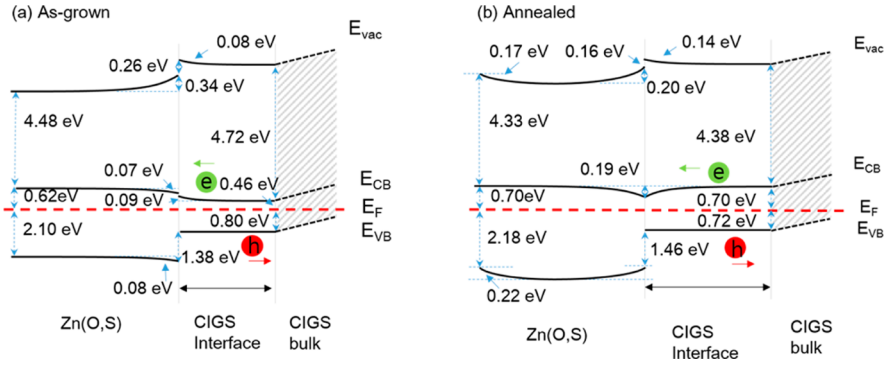

Figure 7. Schematic energy band diagrams of (a) as-grown and (b) annealed Zn(O,S)/CIGS film. E_{VAC}, E_{CB}, E_{VB}, and E_F denote the vacuum level, conduction band edge, valence band edge, and Fermi level.

the as-grown sample. The difference in Ga composition became greater at the front surface than in the CIGS bulk upon annealing. The compositional changes might be possible because the surface energy of In and Ga is lower than other elements.[33] We concluded that Ga could diffuse out to the surface and that Cu could diffuse into the bulk. Similar behavior of the reduction of the Cu content and increase in the Ga and In content has been reported on the surface after air annealing.[34,35] This will be discussed in more detail when we review Figure 7. Determination of both the VB and CB alignments is essential to clarify the interface electronic band structure and to optimize the solar cell junction.

The UPS and IPES spectra as a function of sputtering time for the Zn(O,S)/CIGS samples are shown in Figure 6. Together with the VB region, the VB onsets with vertical bars are displayed in Figure 6, panels a and a′. The characteristic VB shapes of Zn(O,S) and CIGS layers were distinguished by a Zn 3d orbital at 10.6 eV and Cu 3d around 3 eV, respectively.[36] The intensity of the former decreased with sputtering, while the latter increased. The VB onset for the annealed Zn(O,S) layer was slightly higher than that of as-grown Zn(O,S). This difference was indicated by inspection of XPS spectra where the annealed sample showed higher BEs in Zn 2p, O 1s, and S 2s. Figure 6, panels b and b′ show the CB region. For as-grown sample, the CB edge tends to gradually decrease from 0.62 to 0.46 eV with sputtering time. On the other hand, the annealed sample showed a minimal CB edge (0.51 eV) exactly at the Zn(O,S)/CIGS interface. This is related to the relatively small Ga content (Ga/(In+Ga)), as shown in Table 1.[37,38]

The schematic energy band diagrams of both Zn(O,S)/CIGS interfaces with respect to the Fermi level, E_F (red dashed line), are shown in Figure 7. Each CIGS layer shows n-or i-type semiconductor energy band near the interface as the bulk CIGS is p-type by Hall-effect measurement in previous study.[39] The E_F alignment shows that the Zn(O,S)/CIGS interface is composed of a very thin n-or i-type CIGS surface layer created by existing defects related to Cu vacancy, as mentioned earlier in Table 1. This behavior was explained as a substitution of Zn for Cu sites in the CIGS matrix.[40] The interstitial Zn in the CIGS becomes donor and causes charge compensation of p-type CIGS.[41] As a result, the p-type CIGS becomes less p-type. This suggests that the surface layer formed by deposition of Zn(O,S) film at 200 °C forms a buried homojunction. After 400 °C annealing, the high Ga content increases the E_g and conduction band minimum of CIGS film near the interface. Because the annealed Zn(O,S) layer showed a large variation in the S/(S+O) ratio, its VB edge revealed a "bowing" shape, while that of the as-grown Zn(O,S) showed only monotonic band bending. The overall VB level position of the annealed Zn(O,S) layer was located deeper by 0.2 eV than the as-grown sample. Interestingly, the S/(S+O) fluctuation also influenced the CB shape as well. Along with the band modification of the Zn(O,S) layer, the annealing changed the atomic concentration near the interface, as mentioned earlier. That is, the Ga and Zn fractions were enhanced, and the E_g of the CIGS layer became larger. As a result, the minority (electron) carriers moved along CB from the CIGS layer to the Zn(O,S) layer slightly uphill through 0.16 eV band bending for the as-grown sample. In contrast, electrons were trapped in a 0.19 eV potential well ("notch" structure) at the Zn(O,S)/CIGS interface of annealed samples. The notch shape CB is closely related to the Zn(O,S) band bowing as well as to the Cu deficiency and the presence of In-rich content at the very thin interface. Surprisingly, the atomic concentration changes influenced mainly the CB structure of the CIGS layer, while the VB and core level positions remained the same. In fact, because the Zn(O,S) layer is a strong n-type material with a wide E_g, any small variation in VB would not influence the hole blocking function at the interface. Overall, the In and Ga tended to out-diffuse to the top surface and Zn(O,S)/CIGS interface, respectively, while Zn diffused into the interface at high temperature. Such atomic rearrangement modified the energy band alignment at the interface. The notch shape band alignment at the interface CB appeared to act as a trap affecting electron transport and increased the recombination of the charge carriers. This was the main mechanism for device degradation upon annealing.

CONCLUSIONS

To determine the feasibility of the bottom cell in the CIGS tandem structure, solar cell devices of Zn(O,S)/CIGS were heated up to temperatures of 300−500 °C for 60 min in vacuum, similar to the environment in which the top cells are processed. As a result, with the annealing temperature increased to 400 °C, the efficiency of the Zn(O,S)/CIGS solar cell decreased from 11.68% to 7.16% with a drop of V_{OC}. The decrease of EQE in the long wavelengths after 400 °C annealing suggests that there is a surface diffusion layer in the Zn(O,S)/CIGS interface as a result of diffusion of Zn atoms. From the SIMS/TEM results, substantial diffusion of Zn atoms into the CIGS thin film was observed, which could lead to recombination and a CIGS-type conversion. Details of the atomic behavior and electronic structure were obtained from the depth profile provided by the XPS/UPS/IPES measure-

DOI: 10.1021/acsami.5b04815
ACS Appl. Mater. Interfaces 2015, 7, 17425−17432

ments. After 400 °C annealing, the XPS depth profile of the CIGS layer revealed that In and Ga tended to out-diffuse to the surface of the CIGS film and that Zn diffused deeper. This causes a mixed interfacial layer: a small amount of Ga and diffused Zn at the interface induce a slightly increased E_g of CIGS compared to the as-grown sample. Transport properties at heterostructures after annealing treatment were also extracted by describing the band alignment. In the case of sputtered-Zn(O,S) film after 400 °C annealing, the S/(S+O) ratio fluctuated, which could influence the CB shape. Thus, the photoexcited electrons are trapped in a potential well ("notch" structure) formed by modification of the CB shape at the Zn(O,S)/CIGS interface, which resulted in degradation of cell efficiency in case of annealed samples. This study provides a general deterioration mechanism of Zn(O,S)/CIGS interface occurring upon high temperature treatment.

■ ASSOCIATED CONTENT

Supporting Information

Full XRD scans, UV−vis absorption spectrum of $ZnO_{1-x}S_x$ film; I−V characteristics of CIGS solar cell with $ZnO_{1-x}S_x$ buffer layer; and each cell parameters. The Supporting Information is available free of charge on the ACS Publications website at DOI: 10.1021/acsami.5b04815.

■ AUTHOR INFORMATION

Corresponding Author

*E-mail: ydchung@etri.re.kr.

Author Contributions

J.-H.W. and T.G.K. contributed equally to this work.

Notes

The authors declare no competing financial interest.

■ ACKNOWLEDGMENTS

The authors appreciate financial support from the "Development of 25% Efficiency Grade Tandem CIGS Thin Film Solar Cell Core Technology" project of the Ministry of Science, ICT and Future Planning (MSIP), and the Korea Research Council for Industrial Science and Technology (ISTK). This work was also supported by the "New & Renewable Energy Core Technology Program" of the Korea Institute of Energy Technology Evaluation and Planning (KETEP), which granted financial resource from the Ministry of Trade, Industry, and Energy, Republic of Korea (Nos. 20123030010030, 20153010011990). This work was further supported by the Technology Innovation Program (10047001, Exploit ZnS material of long-wave infrared window) funded by the Ministry of Trade, Industry, and Energy (MOTIE).

■ REFERENCES

(1) Jackson, P.; Hariskos, D.; Wuerz, R.; Kiowski, O.; Bauer, A.; Friedlmeier, T. M.; Powalla, M. Properties of Cu(In,Ga)Se_2 Solar Cells with New Record Efficiencies up to 21.7%. *Phys. Status Solidi RRL* **2015**, *9*, 28−31.

(2) Cho, D.-H.; Lee, W.-J.; Park, S.-W.; Wi, J.-H.; Han, W. S.; Kim, J.; Cho, M.-H.; Kim, D.; Chung, Y.-D. Non-toxically Enhanced Sulfur Reaction for Formation of Chalcogenide Thin Films Using a Thermal Cracker. *J. Mater. Chem. A* **2014**, *2*, 14593−14599.

(3) Okamoto, A.; Minemoto, T.; Takakura, H. Application of Sputtered $ZnO_{1-x}S_x$ Buffer Layers for Cu(In,Ga)Se_2 Solar Cells. *Jpn. J. Appl. Phys.* **2011**, *50*, 04DP10.

(4) Nakashima, K.; Kumazawa, T.; Kobayashi, T.; Mise, T.; Nakada, T. Wide-gap Cu(In,Ga)Se_2 Solar Cells with Zn(O,S) Buffer Layers Prepared by Atomic Layer Deposition. *Jpn. J. Appl. Phys.* **2012**, *51*, 10NC15.

(5) Platzer-Bjorkman, C.; Torndahl, T.; Abou-Ras, D.; Malmstrom, J.; Kessler, J.; Stolt, L. Zn(O,S) Buffer Layers by Atomic Layer Deposition in Cu(In,Ga)Se_2 Based Thin Film Solar Cells: Band Alignment and Sulfur Gradient. *J. Appl. Phys.* **2006**, *100*, 044506−044509.

(6) Wi, J.-H.; Lee, W.-J.; Cho, D.-H.; Han, W. S.; Yun, J. H.; Chung, Y.-D. Characteristics of Temperature and Wavelength Dependence of $CuInSe_2$ Thin-Film Solar Cell with Sputtered Zn(O,S) and CdS Buffer Layers. *Phys. Status Solidi A* **2014**, *211*, 2172−2176.

(7) Pettersson, J.; Platzer-Björkman, C.; Edoff, M. Temperature-Dependent Current-Voltage and Light Soaking Measurements on Cu(In,Ga)Se_2 Solar Cells with ALD-$Zn_{1-x}Mg_xO$ Buffer Layers. *Prog. Photovoltaics* **2009**, *17*, 460−469.

(8) Lindahl, J.; Wätjen, J. T.; Hultqvist, A.; Ericson, T.; Edoff, M.; Törndahl, T. The Effect of $Zn_{1-x}Sn_xO_y$ Buffer Layer Thickness in 18.0% Efficient Cd-free Cu(In,Ga)Se_2 Solar Cells. *Prog. Photovoltaics* **2013**, *21*, 1588−1597.

(9) Chung, Y.-D.; Cho, D.-H.; Park, N.-M.; Lee, K.-S.; Kim, J. Effect of Annealing on CdS/Cu(In,Ga)Se_2 Thin-Film Solar Cells. *Curr. Appl. Phys.* **2011**, *11*, S65−S67.

(10) Bastek, J.; Stolwijk, N. A.; Wuerz, R.; Eicke, A.; Albert, J.; Sadewasser, S. Zinc Diffusion in Polycrystalline Cu(In,Ga)Se_2 and Single-Crystal $CuInSe_2$ Layers. *Appl. Phys. Lett.* **2012**, *101*, 074105−074101.

(11) Hiepko, K.; Bastek, J.; Schlesiger, R.; Schmitz, G.; Wuerz, R.; Stolwijk, N. A. Diffusion and Incorporation of Cd in Solar-Grade Cu(In,Ga)Se_2 Layers. *Appl. Phys. Lett.* **2011**, *99*, 234101−234103.

(12) Shafarman, W. N.; Paulson, P. D. Losses in $CuInSe_2$-Based Thin Film Monolithic Tandem Solar Cells. *Proc. 31st IEEE Photovoltaic Specialist Conf.* **2005**, 231−234.

(13) Shin, D. H.; Kim, S. T.; Kim, J. H.; Kang, H. J.; Ahn, B. T.; Kwon, H. Study of Band Structure at the Zn(S,O,OH)/Cu(In,Ga)Se_2 Interface via Rapid Thermal Annealing and their Effect on the Photovoltaic Properties. *ACS Appl. Mater. Interfaces* **2013**, *5*, 12921−12927.

(14) Nakada, T.; Mizutani, M. *Improved Efficiency of Cu(In,Ga)Se_2 Thin Film Solar Cells with Chemically Deposited ZnS Buffer Layers by Air-Annealing-Formation of Homojunction by Solid Phase Diffusion*; Proceedings of the 28th IEEE Photovoltaic Specialists Conference, 2000; pp 529−534. DOI: 10.1109/PVSC.2000.915889.

(15) Witte, W.; Hariskos, D.; Eicke, A.; Menner, R.; Kiowski, O.; Powalla, M. Impact of Annealing on Cu(In,Ga)Se_2 Solar Cells with Zn(O,S)/(Zn,Mg)O Buffers. *Thin Solid Films* **2013**, *535*, 180−183.

(16) Chung, Y.-D.; Cho, D.-H.; Han, W.-S.; Park, N.-M.; Lee, K.-S.; Kim, J. Incorporation of Cu in Cu(In,Ga)Se_2-based Thin-film Solar Cells. *J. Korean Phys. Soc.* **2010**, *57*, 1826−1830.

(17) Cho, D.-H.; Chung, Y.-D.; Lee, K.-S.; Park, N.-M.; Kim, K.-H.; Choi, H.-W.; Kim, J. Influence of Growth Temperature of Transparent Conducting Oxide Layer on Cu(In,Ga)Se_2 Thin-Film Solar Cells. *Thin Solid Films* **2012**, *520*, 2115−2118.

(18) Lavreko, T.; Walter, T.; Steigert, A.; Klenk, R. *Stability Issues of Sputtered Zn(O,S) Buffer Layers for CIGS Thin Film Solar Cells*; 28th European Photovoltaic Solar Energy Conference (EU PVSEC): Paris, France, September 30−October 4, 2013; pp 2393−2397. DOI: 10.4229/28thEUPVSEC2013-3BV.6.22.

(19) Kim, J. W. *Photodetector Included Microchannel Plate, Method for Detecting Photo, Analysis System for Analyzing Sample and Method There of.* Korea Patent 10−2010−0099582, 2010.

(20) Lee, H.; Lee, J.; Park, S.; Yi, Y.; Cho, S. W.; Kim, J. W.; Kang, S. J. Hole Injection Enhancement of a Single-Walled Carbon Nanotube Anode Using an Organic Charge-Generation Layer. *Carbon* **2014**, *71*, 268−275.

(21) Baars, J.; Brandt, G. Structural Phase Transitions in ZnS. *J. Phys. Chem. Solids* **1973**, *34*, 905−909.

(22) Meyer, B. K.; Polity, A.; Farangis, B.; He, Y.; Hasselkamp, D.; Kramer, T.; Wang, C. Structural Properties and Bandgap Bowing of

DOI: 10.1021/acsami.5b04815
ACS Appl. Mater. Interfaces 2015, 7, 17425−17432

$ZnO_{1-x}S_x$ Thin Films Deposited by Reactive Sputtering. *Appl. Phys. Lett.* **2004**, *85*, 4929−4931.
(23) Yoo, Y.-Z.; Jin, Z.-W.; Chikyow, T.; Fukumura, T.; Kawasaki, M.; Koinuma, H. S Doping in ZnO Film by Supplying ZnS Species with Pulsed-Laser-Deposition Method. *Appl. Phys. Lett.* **2002**, *81*, 3798−3800.
(24) Locmelis, S.; Brünig, C.; Binnewies, M.; Börger, A.; Becker, K. D.; Homann, T.; Bredow, T. Optical Band Gap in the System $ZnO_{1-x}S_x$. An Experimental and Quantum Chemical Study. *J. Mater. Sci.* **2007**, *42*, 1965−1971.
(25) Lin, P.-C.; Hua, C. C.; Lee, T.-C. Low-Temperature Phase Transition of ZnS: The Critical Role of ZnO. *J. Solid State Chem.* **2012**, *194*, 282−285.
(26) Pan, H. L.; Yang, T.; Yao, B.; Deng, R.; Sui, R. Y.; Gao, L. L.; Shen, D. Z. Characterization and Properties of $ZnO_{1-x}S_x$ Alloy Films Fabricated by Radio-Frequency Magnetron Sputtering. *Appl. Surf. Sci.* **2010**, *256*, 4621−4625.
(27) von Wenckstern, H.; Schmidt, H.; Brandt, M.; Lajn, A.; Pickenhain, R.; Lorenz, M.; Grundmann, M.; Hofmann, D. M.; Polity, A.; Meyer, B. K.; Saal, H.; Binnewies, M.; Börger, A.; Becker, K. D.; Tikhomirov, V. A.; Jug, K. Anionic and Cationic Substitution in ZnO. *Prog. Solid State Chem.* **2009**, *37*, 153−172.
(28) Persson, C.; Platzer-Björkman, C.; Malmström, J.; Törndahl, T.; Edoff, M. Strong Valence-Band Offset Bowing of $ZnO_{1-x}S_x$ Enhances p-Type Nitrogen Doping of ZnO-like Alloys. *Phys. Rev. Lett.* **2006**, *97*, 146403−146406.
(29) Grimm, A.; Just, J.; Kieven, D.; Lauermann, I.; Palm, J.; Neisser, A.; Rissom, T.; Klenk, R. Sputtered Zn(O,S) for Junction Formation in Chalcopyrite-Based Thin Film Solar Cells. *Phys. Status Solidi RRL* **2010**, *4*, 109−111.
(30) Hu, X.; Masuda, Y.; Ohji, T.; Kato, K. Fabrication of $Zn(OH)_2$/ZnO Nanosheet-ZnO Nanoarray Hybrid Structured Films by a Dissolution-Recrystallization Route. *J. Am. Ceram. Soc.* **2010**, *93*, 881−886.
(31) Zhang, X.; Qin, J.; Xue, Y.; Yu, P.; Zhang, B.; Wang, L.; Liu, R. Effect of Aspect Ratio and Surface Defects on the Photocatalytic Activity of ZnO Nanorods. *Sci. Rep.* **2014**, *4*, 4596−4603.
(32) Uhm, G.-R.; Jang, S. Y.; Jeon, Y. H.; Yoon, H. K.; Seo, H. Optimized Electronic Structure of a $Cu(In,Ga)Se_2$ Solar Cell with Atomic Layer Deposited Zn(O,S) Buffer Layer for High Power Conversion Efficiency. *RSC Adv.* **2014**, *4*, 28111−28118.
(33) Cao, Q.; Gunawan, O.; Copel, M.; Reuter, K. B.; Chey, S. J.; Deline, V. R.; Mitzi, D. B. Defects in Chalcopyrite Semiconductors: Defects in $Cu(In,Ga)Se_2$ Chalcopyrite Semiconductors: A Comparative Study of Material Properties, Defect States, and Photovoltaic Performance. *Adv. Energy Mater.* **2011**, *1*, 844−853.
(34) Rau, U.; Braunger, D.; Herberholz, R.; Schock, H. W.; Guillemoles, J.-F.; Kronik, L.; Cahen, D. Oxygenation and Air-Annealing Effects on the Electronic Properties of $Cu(In,Ga)Se_2$ Films and Devices. *J. Appl. Phys.* **1999**, *86*, 497−505.
(35) Shin, Y. M.; Lee, C. S.; Shin, D. H.; Kwon, H. S.; Park, B. G.; Ahn, B. T. Surface Modification of CIGS Film by Annealing and Its Effect on the Band Structure and Photovoltaic Properties of CIGS Solar Cells. *Curr. Appl. Phys.* **2015**, *15*, 18−24.
(36) Park, S. M.; Kim, T. G.; Chung, Y. D.; Cho, D.-H.; Kim, J.; Kim, K. J.; Yi, Y.; Kim, J. W. Junction Formation at the Interface of CdS/$CuIn_xGa_{(1-x)}Se_2$. *J. Phys. D: Appl. Phys.* **2014**, *47*, 345302−345309.
(37) Chirila, A.; Buecheler, S.; Pianezzi, F.; Bloesch, P.; Gretener, C.; Uhl, A. R.; Fella, C.; Kranz, L.; Perrenoud, J.; Seyrling, S.; Verma, R.; Nishiwaki, S.; Romanyuk, Y. E.; Bilger, G.; Tiwari, A. N. Highly Efficient $Cu(In,Ga)Se_2$ Solar Cells Grown on Flexible Polymer Films. *Nat. Mater.* **2011**, *10*, 857−861.
(38) Sharbati, S.; Sites, J. R. Impact of the Band Offset for n-Zn(O,S)/p-$Cu(In,Ga)Se_2$ Solar Cells. *IEEE J. Photovoltaics.* **2014**, *4*, 697−702.
(39) Cho, D.-H.; Lee, K.-S.; Chung, Y.-D.; Kim, J.-H.; Park, S.-J.; Kim, J. Electronic Effect of Na on $Cu(In,Ga)Se_2$ Solar Cells. *Appl. Phys. Lett.* **2012**, *101*, 023901−023904.
(40) Nakada, T.; Kunioka, A. Direct Evidence of Cd Diffusion into $Cu(In, Ga)Se_2$ Thin Films during Chemical-Bath Deposition Process of CdS Films. *Appl. Phys. Lett.* **1999**, *74*, 2444−2446.
(41) Lee, C.-S.; Kim, S.; Al-Ammar, E. A.; Kwon, H.; Ahn, B. T. Effects of Zn Diffusion from (Zn,Mg)O Buffer to CIGS Film on the Performance of Cd-Free $Cu(In,Ga)Se_2$ Solar Cells. *ECS J. Solid State Sci. Technol.* **2014**, *3*, Q99−Q103.

DOI: 10.1021/acsami.5b04815
ACS Appl. Mater. Interfaces 2015, 7, 17425−17432